I&EC research
Industrial & Engineering Chemistry Research

Article

Cite This: Ind. Eng. Chem. Res. 2019, 58, 1743−1753

pubs.acs.org/IECR

Water Sorption and Diffusivity in $[C_2C_1im][BF_4]$, $[C_4C_1im][OAc]$, and $[C_4C_1im][Cl]$

M. Alejandra Rocha and Mark B. Shiflett*

Department of Chemical and Petroleum Engineering, University of Kansas, 1450 Jayhawk Boulevard, Lawrence, Kansas 66045, United States

Supporting Information

ABSTRACT: Measurements of in situ atmospheric water absorption and desorption in ionic liquids (ILs) (1-ethyl-3-methylimidazolium tetrafluoroborate $[C_2C_1im][BF_4]$, 1-butyl-3-methylimidazolium acetate $[C_4C_1im][OAc]$, and 1-butyl-3-methylimidazolium chloride $[C_4C_1im][Cl]$) were made using a gravimetric microbalance at temperatures ranging from 283.15 to 315.15 K and relative humidity (RH) 0−70% at 101 kPa. Solubility data were well correlated using the nonrandom two-liquid (NRTL) activity model, and time dependent concentration data were used to determine the binary diffusion coefficients using one- and two-dimensional transport models of water in the IL−water systems. The solubility of water was highest in $[C_4C_1im][OAc]$ (77.5 mol %), followed by $[C_4C_1im][Cl]$ (68.6 mol %), and $[C_2C_1im][BF_4]$ (19.5 mol %) at equivalent conditions (303.15 K and 25.00% RH). The diffusion coefficients in order of increasing relative humidity ranged from 1.3×10^{-10} to 2.8×10^{-11} m^2/s for $[C_2C_1im][BF_4]$, from 8.8×10^{-12} to 3.9×10^{-11} m^2/s for $[C_4C_1im][OAc]$, and from 4.5×10^{-12} to 2.8×10^{-11} m^2/s for $[C_4C_1im][Cl]$. Heats of absorption were calculated and ranged from 39 to 44 kJ/mol for $[C_2C_1im][BF_4]$, from 47 to 45 kJ/mol for $[C_4C_1im][OAc]$, and from 55 to 45 kJ/mol for $[C_4C_1im][Cl]$ with increasing water mole fraction of 0.3−0.8. The water diffusivity increases with increasing water concentration in both $[C_4C_1im][OAc]$ and $[C_4C_1im][Cl]$ with respect to decreasing viscosity and heats of absorption. However, the diffusivity of water in $[C_2C_1im][BF_4]$ decreases with increasing water concentration with respect to decreasing viscosity and increasing heats of absorption. Diffusing radius calculations using the Stokes−Einstein relationship support the hypothesis that a few water molecules through hydrogen bonding form clusters with the [OAc] and [Cl] anions, but much larger water/BF_4^- clusters/networks are occurring in the $[C_2C_1im][BF_4]$ system which increase in size with increase in water concentration.

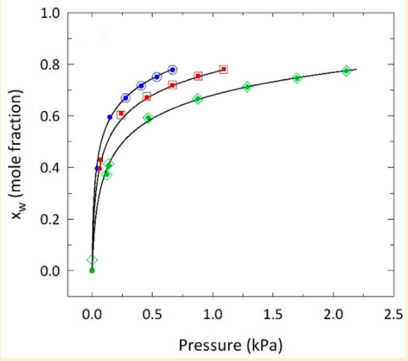

I. INTRODUCTION

Ionic liquids (ILs) are organic salts which are liquid at temperatures below 373.15 K. Studies involving ILs continue to increase, with more than 5000 papers published on the topic by 2016.[1] Part of the interest in ILs is due to their negligible vapor pressure and the ability to tailor both the cation and anion, which allows them to replace conventional organic solvents and be designed for specific applications. However, the tunable physical and chemical properties of ILs, such as viscosity, density, conductivity, and solvation ability, can be affected by water contamination.[2−4] Depending on the application, the effect of water present in ionic liquids may be beneficial, as it is in improving extraction of proteins.[5] Yet in other cases, the presence of water in ILs can be detrimental, such as hindering the solvation of cellulose,[6] or reducing the electrochemical window[7] and making the use of ILs impractical as electrolyte materials. Although ionic liquids can conventionally be separated into hydrophobic or hydrophilic categories, all ILs are hygroscopic to an extent.[8−10] Most studies investigating water−IL interactions are performed with deliberate water addition to the IL system. However, the most common and realistic methods of undesired water sorption occur from exposure to atmospheric conditions.

The present study investigates the in situ atmospheric water vapor absorption and desorption in three imidazolium-based ionic liquids: $[C_2C_1im][BF_4]$, $[C_4C_1im][OAc]$, and $[C_4C_1im][Cl]$ over a range of temperatures (283−315 K) and relative humidity conditions (0−70%). The isothermal measurements were performed using a gravimetric microbalance, which measured total weight as a function of time. The IL $[C_2C_1im][BF_4]$ was selected in order to validate the gravimetric technique used herein, and $[C_4C_1im][OAc]$ and $[C_4C_1im][Cl]$ were chosen as these are known hydrophilic ionic liquids. The solubility data was correlated using the nonrandom two-liquid (NRTL) solution model, and the time-dependent mass sorption data was analyzed to calculate diffusion coefficients and enthalpies of absorption.

Received: November 15, 2018
Revised: January 5, 2019
Accepted: January 7, 2019
Published: January 7, 2019

DOI: 10.1021/acs.iecr.8b05689
Ind. Eng. Chem. Res. 2019, 58, 1743−1753

II. EXPERIMENTAL METHODS

II.a. Materials. The ionic liquids (ILs) investigated in this work were 1-ethyl-3-methylimidazolium tetrafluoroborate [C_2C_1im][BF_4] (≥98.5% purity, Fluka, lot and filling code 1084445 11106247, CAS No. 143314-16-3), 1-butyl-3-methylimidazolium acetate [C_4C_1im][OAc] (>95% purity, Fluka, lot and filling code S41687 11707B11, CAS No. 284049-75-8), and 1-butyl-3-methylimidazolium chloride [C_4C_1im][Cl] (>99.0% purity, lot and filling code 1084617 22905013, CAS No. 79917-90-1). The as-received water content was determined for each ionic liquid using Karl Fischer coulometric titration (Mettler Toledo DL36 Karl Fischer coulometric titrator), and the calibration was checked with a water standard (94 ± 10 ppm H_2O, Apura , Merck KGaA, product no. 1.88050.0010, lot code HC61276950). Water concentrations in [C_2C_1im][BF_4], [C_4C_1im][OAc], and [C_4C_1im][Cl] were determined to be 249 ± 13 ppm, 2200 ± 400 ppm, and 4636 ± 53 ppm, respectively. The chemical structures of the ILs are shown in Figure 1.

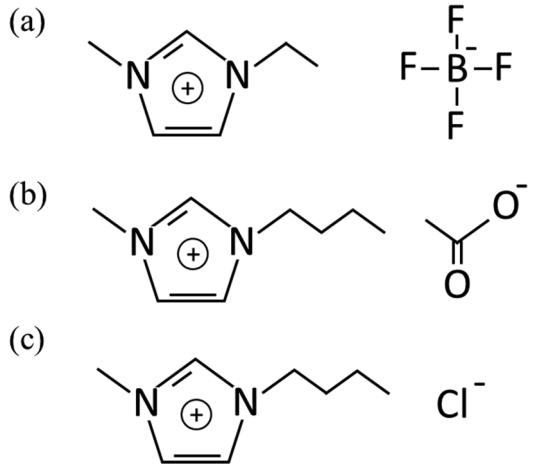

Figure 1. Chemical structures of ILs studied: (a) [C_2C_1im][BF_4], (b) [C_4C_1im][OAc], and (c) [C_4C_1im][Cl].

The sorption studies used reverse osmosis water (15 mΩ·cm at 298 K) and nitrogen gas (Matheson grade <1 ppm H_2O, lot code 7727-37-9), and a molecular sieve trap (Restek 22015, lot code 393152-22015) was installed at the inlet to the microbalance instrument to remove trace amounts of water from the nitrogen gas.

II.b. Absorption and Desorption Studies. *II.b.i. Instrument Overview.* Water sorption experiments were measured gravimetrically using the Hiden Isochema IGAsorp microbalance. The IGAsorp is a dynamic vapor analyzer, with a 0.05 μg resolution and a 1 g weighing capacity limit. It operates at ambient pressure with a temperature range of 278−573 K and has a sample side and a counterweight side, as illustrated in Figure 2 with components listed in Table 1. The instrument measures the mass of the sample as a function of time, and the data acquisition and control is via the Hiden HIsorp software.

The IGAsorp operates in dynamic mode and utilizes a combination of wet and dry nitrogen streams to control the relative humidity (RH) inside the instrument. The RH sensor (Vaisala HMT333, ±1% RH) located in the sample chamber provides feedback to the mass flow controllers, and the temperature probe (platinum RTD ±0.1 K) provides feedback to the water bath and/or heater. A detailed description of the

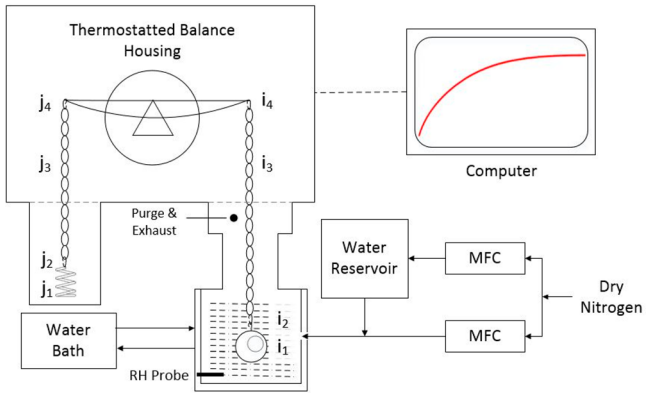

Figure 2. Diagram of the IGAsorp gravimetric microbalance. Counterweight and sample side components (symbols "i" and "j") are described in Table 1.

instrument operation and experimental procedure has been published;[11] however, it is worthwhile to describe the buoyancy correction applied in this study. The buoyant force (C_b) acting on an object can be calculated using eq 1, where g is the gravitational acceleration, V_i is the object volume, and ρ_g is the density of the gas surrounding the object at a known temperature and relative humidity (T, RH).

$$C_b = gV_i\rho_g(T, \text{RH}) \tag{1}$$

The density of the gas surrounding the sample container is calculated using the partial pressures of nitrogen (P_{N_2}) and water (P_{H_2O}), as shown in eq 2.

$$\rho_g = \frac{P_{H_2O}MW_{H_2O} + P_{N_2}MW_{N_2}}{RT} \tag{2}$$

The partial pressure of water is related to the relative humidity and temperature, as shown in eq 3, where P^0 is the saturation pressure of water. The NIST database (REFPROP v9.1[12]) was used to determine physical properties for nitrogen and water used in this study.

$$\%\text{RH} = \frac{P_{H_2O}}{P^0_{H_2O}(T)} \times 100\% \tag{3}$$

Prior to loading the sample, a force balance is used to determine the correction factor needed to minimize the buoyancy effects.[11] The force balance shown in eq 4 includes the summation of the sample side (m_i, m_s, m_a), and counterweight side components (m_j), the summation of the buoyancy effects on both the sample side and counterweight side, and the correction factor (C_f). The force balance also includes physical properties such as component density for each item on the sample and tare weight sides (ρ_{i_k} and ρ_{j_k}), surrounding gas density (ρ_g), sample density (ρ_s), and absorbed mass density (ρ_a). As shown in eq 4 and Table 1, temperature within the balance is a function of position. The balance housing is controlled and maintained at 343.15 K, the counterweight side is not temperature controlled but is often at approximately 333.15 K, and the sample chamber temperature is controlled using the water bath or the heater. Therefore, a temperature profile is present along both sides of the balance, as reported in Table 1.

DOI: 10.1021/acs.iecr.8b05689
Ind. Eng. Chem. Res. 2019, 58, 1743−1753

Table 1. IGAsorp Components Considered in the Buoyancy Correction for This Study

symbol	component	material	weight (g)	density (g/cm^3)	temperature (K)
s	sample	variable	m_s	ρ_s	sample temp
a	interacted vapor	water	m_a	ρ_a	sample temp
i_1	sample container	Pyrex	0.271	2.23	sample temp
i_2	lower sample hook	tungsten	0.0057	19.04	sample temp
i_3	sample chain	22 kt gold	0.0930	11.10	temp profile *i*
i_4	sample side balance hook	tungsten	0.0059	19.04	343.15
j_1	counterweight (CW)	316 SS	0.3808	7.89	333.15
j_2	lower CW hook	tungsten	0.0057	19.04	333.15
j_3	CW chain	22 kt gold	0.0650	11.10	top half = 338.15; bottom half = 333.15
j_4	CW side balance hook	tungsten	0.0058	1.04	343.15

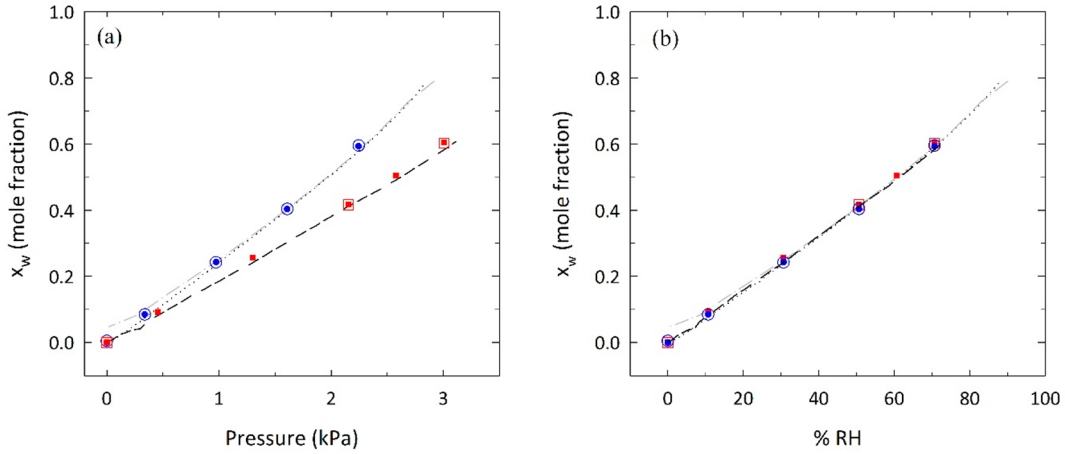

Figure 3. Measured absorption and desorption isotherms of water in $[C_2C_1im][BF_4]$ at 298.15 and 303.15 K as (a) a function of partial pressure of water and (b) a function of relative humidity. Data at 298.15 K are shown in blue circles, and data at 303.15 K are shown in red squares. Filled symbols represent absorption, and open symbols represent desorption. Uncertainties for the data measured in this work were determined to be <0.1 mol %. Black dotted and dashed lines are the fitted absorption data measured by Takamuku et al.,[13] and the gray dashed line is the fitted desorption data by Takamuku et al.[13] Tabulated data can be found in the Supporting Information.

$$m_{\mathrm{IGAsorp}} = \sum_{k=1}^{4} m_{i_k} + m_s + m_a - \sum_{k=1}^{4} \frac{m_{i_k}}{\rho_{i_k}} \rho_g(T_{i_k}, \mathrm{RH}) - \frac{m_s}{\rho_s} \rho_g(T_s, \mathrm{RH}) - \frac{m_a}{\rho_a} \rho_g(T_a, \mathrm{RH}) - \left(\sum_{k=1}^{4} m_{j_k} - \sum_{k=1}^{4} \frac{m_{j_k}}{\rho_{j_k}} \rho_g(T_{j_k}, \mathrm{RH}) \right) - C_f(T_s, \mathrm{RH}) \quad (4)$$

The correction factor (C_f) is determined using eq 4 when there is no sample in the sample container, i.e., when m_s and m_a are zero. Finally, the mass absorbed (m_a) can now be accurately calculated as a function of T and RH corrected for buoyancy.

II.b.ii. Sorption Isotherms. Approximately 60 mg of IL was loaded into a clean Pyrex glass bulb (12.73 mm diameter) at room temperature (295 ± 1 K) and room humidity (40 ± 1%) and placed in the IGAsorp. This was done as quickly as possible to minimize absorption of atmospheric water into the ionic liquid (<5 min). Prior to every isotherm experiment, a pretreatment isotherm was performed at 348.15 ± 0.1 K and 0% RH for 15 h in the IGAsorp to remove any traces of residual water. Two isotherms were measured for $[C_2C_1im][BF_4]$ + H_2O system at 298.15 ± 0.1 K and 303.15 ± 0.1 K and 0, 10.67 ± 1.00, 30.67 ± 1.00, 50.67 ± 1.00, and 70.67 ± 1.00% RH. A comparison was made with the $[C_2C_1im][BF_4]$ data to previously published results by Takamuku et al.[13] to check the reproducibility of the methods.

Three isotherms were measured for the $[C_4C_1im][OAc]$ + H_2O system at 294.85 ± 0.01 K, 303.15 ± 0.01 K, and 315.15 ± 0.01 K and 0, 1.47 ± 1.00, 1.67 ± 1.00, 5.67 ± 1.00, 10.67 ± 1.00, 15.67 ± 1.00, 20.67 ± 1.00, and 25.67 ± 1.00% RH; however, at 294.85 K the 1.47% RH measurement was not possible because this would require the reservoir of water to be at a temperature below its lower temperature limit (298 K). A detailed description of the IGAsorp procedure for operating at low RH has been published.[11] Three isotherms were also measured for the $[C_4C_1im][Cl]$ system at 283.15 ± 0.01 K, 295.15 ± 0.01 K, and 303.15 ± 0.01 K and 0, 1.67 ± 1.00, 5.67 ± 1.00, 10.67 ± 1.00, 15.67 ± 1.00, 20.67 ± 1.00, and 25.67 ± 1.00% RH. The reader many note that the RH values, with the exception of 0% RH, were 0.67% RH higher than the specified set point value which was due to a calibration correction for the RH probe.

Each relative humidity set point had a minimum time-out of 3 h and, in some cases, a maximum time-out of 100 h to allow enough time for vapor−liquid equilibrium to be achieved. The IGAsorp software, HIsorp, can also predict the equilibrium water solubility using real-time mass vs time data. The HIsorp software uses the linear driving force (LDF) model shown in eq 5.

$$y = y_0 + \Delta y[1 - e^{-(t-t_0)k}] \quad (5)$$

DOI: 10.1021/acs.iecr.8b05689
Ind. Eng. Chem. Res. 2019, 58, 1743−1753

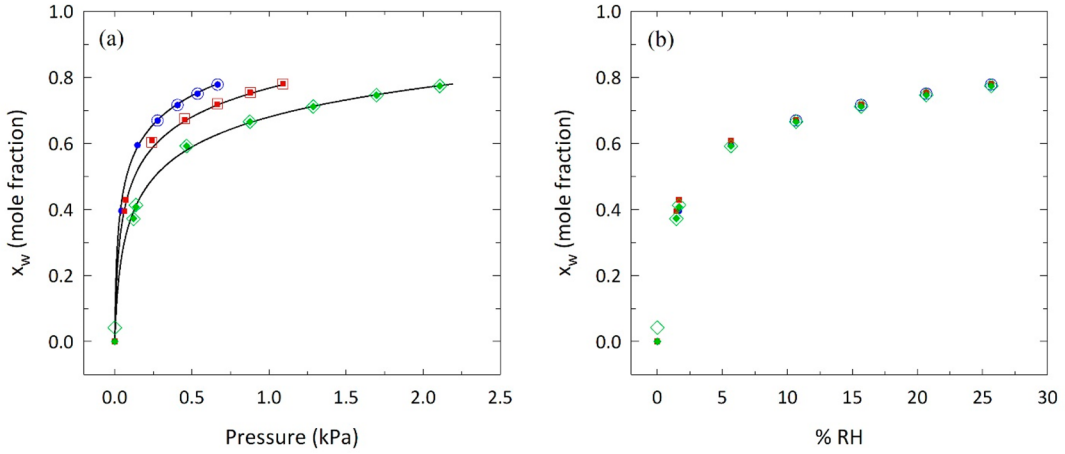

Figure 4. Measured absorption and desorption isotherms of water in $[C_4C_1im][OAc]$ at 294.85, 303.15, and 315.15 K as (a) a function of partial pressure of water and (b) a function of relative humidity. Blue circles represent data at 294.85 K; red squares represent data at 303.15 K; green diamonds represent data at 315.15 K. Filled symbols represent absorption, and open symbols represent desorption. The black solid lines in (a) are calculated with the NRTL equation. Uncertainties were <0.1 mol %. Tabulated data can be found in the Supporting Information.

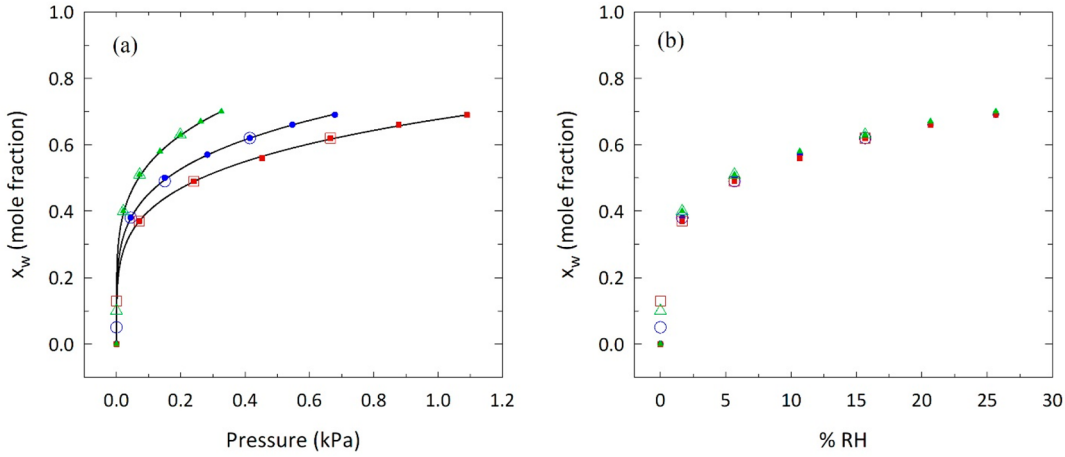

Figure 5. Measured absorption and desorption isotherms of water in $[C_4C_1im][Cl]$ at 283.15, 295.15, and 303.15 K as (a) a function of partial pressure of water and (b) a function of relative humidity. Green triangles represent data at 283.15 K; blue circles represent data at 295.15 K; red squares represent data at 303.15 K. Filled symbols represent absorption and open symbols represent desorption. The solid black lines in (a) are calculated with the NRTL equation. Uncertainties were <0.1 mol %. Tabulated data can be found in the Supporting Information.

The LDF model fits the measured mass of the sample y (mg) as a function of time t (min) using four adjustable parameters: k is the kinetic rate constant (min^{-1}), Δy (mg) is the difference between the mass at equilibrium and the initial mass, y_0 (mg) is the initial mass, and, when y_0 is selected, the t_0 initial time (min) is also defined. At low T and high % RH conditions, equilibrium could take more than 50 h, so the LDF model was used to predict the absorption/desorption solubility. The slow sorption was expected due to the high viscosity of the ionic liquids and the ambient pressure driving force, and most importantly, there was no mixing, such that the equilibrium was purely diffusion-driven with no convection. It should be noted that it took approximately 2 months to measure each H_2O + IL system.

III. RESULTS AND DISCUSSION

III.a. Solubility and Data Comparison. Experimental data for the absorption and desorption of $[C_2C_1im][BF_4]$ were compared to data previously measured by Takamuku et al.[13] using a similar method. A comparison of the data is shown in Figure 3, and the results are in close agreement (%AARD (average absolute relative deviation) < 4.6%). The slight deviation observed between the results at higher humidity can be attributed to the buoyancy correction applied in the current analysis. Figure 3a provides a comparison of the solubility of water as a function of the partial pressure of water. The absorption and desorption data show no indication of hysteresis, indicating the sorption mechanism of water into $[C_2C_1im][BF_4]$ is physical. When the solubility results are plotted as a function of percent relative humidity (% RH) (Figure 3b), the isotherms converge and overlap as expected. An important difference to mention is the measurements performed by Takamuku et al.[13] were carried out using a magnetic suspension balance with only water vapor and no inert carrier gas, such as nitrogen which was used in the present method. The close agreement in the two methods confirms that using nitrogen as a carrier gas has little to no significant effect on the solubility and that the IGAsorp is an accurate and reliable technique for measuring water sorption in ionic liquids. This was to be expected due to the very low solubility of N_2 in $[C_2C_1im][BF_4]$ (0.001 mole fraction N_2 at

DOI: 10.1021/acs.iecr.8b05689
Ind. Eng. Chem. Res. 2019, 58, 1743−1753

298.15 K and 101 kPa[14]). The solubility of N_2 in $[C_4C_1im][OAc]$ and $[C_4C_1im][Cl]$ was expected to also be within the same range, and therefore was considered negligible.[15]

The absorption and desorption of water in $[C_4C_1im][OAc]$ and $[C_4C_1im][Cl]$ as a function of water partial pressure and % RH are shown in Figures 4 and 5, respectively. As expected, the concentration of water in the ionic liquids increases with increasing relative humidity (or partial water vapor pressure) and decreases with increasing temperature as shown in Figures 3–5. In addition, there is little to no difference between absorption and desorption measurements as shown in Figures 3a, 4a, and 5a, which indicates that the sorption process is reversible and indicates physical sorption. When the solubility data are plotted as a function of % RH, the isotherms converge and overlap, as shown in Figures 3b, 4b, and 5b. As expected, the absorption of water depends only on the relative humidity which incorporates the effect of temperature via P^0 (saturation pressure of water) as shown in eq 3.

A clear difference can be observed in the shape of the isotherms for each IL–water system as shown in Figure 6. The isotherms for the H_2O + $[C_2C_1im][BF_4]$ system are essentially linear over the relative humidity range measured (0–70% RH), while the isotherms for the H_2O + $[C_4C_1im][OAc]$ and H_2O + $[C_4C_1im][Cl]$ systems exhibit typical Langmuir-type isothermal behavior. The $[C_4C_1im][OAc]$ and $[C_4C_1im][Cl]$ ionic liquids absorbed a higher amount of water than $[C_2C_1im][BF_4]$, even at much lower relative humidity (i.e., 25% RH). This illustrates the expected higher water absorption capacity of $[C_4C_1im][OAc]$ and $[C_4C_1im][Cl]$.

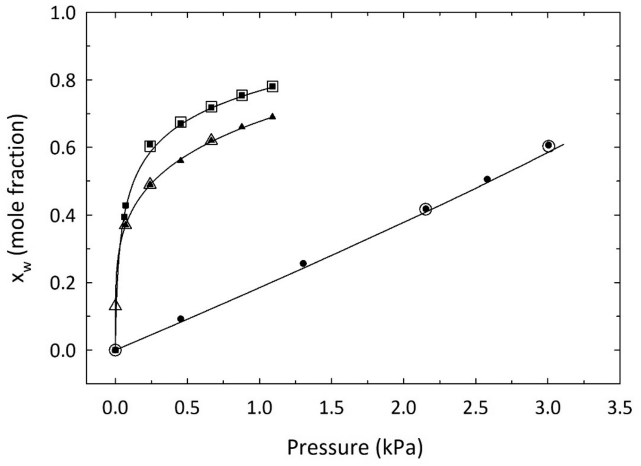

Figure 6. Solubility data comparison for $[C_2C_1im][BF_4]$ (circles), $[C_4C_1im][OAc]$ (squares), and $[C_4C_1im][Cl]$ (triangles) at 303.15 K. Filled symbols represent absorption, and open symbols represent desorption. The solid black lines are calculated with the NRTL equation. The NRTL fit for $[C_2C_1im][BF_4]$ was developed using experimental data from Takamuku et al.[13]

III.b. Thermodynamic Modeling. The solubility of water in the three ionic liquids was modeled using the NRTL activity coefficient model which has been used successfully to fit other water–ionic liquid systems.[16−18] The NRTL model can be applied to the current systems because the measured pressures are low ($P \leq 101.325$ kPa) and the vapor pressure for the ionic liquid is assumed to be negligible ($P_2 = 0$). The calculation begins with the vapor–liquid equilibrium of a binary mixture (eq 6), where i represents the species (1) water and (2) IL, γ is the activity coefficient, x is the mole fraction of i in the liquid phase, f/P is the fugacity coefficient, and y is the mole fraction of i in the gas phase.

$$\sum_{i=1}^{2} x_i\gamma_i(T, P, x)P_i^{sat}(T)\left(\frac{f}{P}\right)_{sat,i} = P\sum_{i=1}^{2} y_i\left(\frac{f}{P}\right)_i \tag{6}$$

Equation 6 can be simplified assuming the absorption of nitrogen into ionic liquids is insignificant, the vapor pressures of ILs are negligible, and, due to the sufficiently low pressures, the fugacity coefficient corrections are essentially equal to 1. This results in the simplified equation (eq 7):

$$x_1\gamma_1P_1^{sat} = P_1 \tag{7}$$

The activity coefficient can be calculated using the NRTL model as shown in eq 8, where τ_{12} and τ_{21} are the dimensionless interaction parameters.

$$P_1 = P_1^{sat}x_1\exp\left(x_2^2\left(\tau_{21}\left(\frac{G_{21}}{x_1 + x_2G_{21}}\right)^2 + \frac{\tau_{12}G_{12}}{(x_2 + x_1G_{12})^2}\right)\right) \tag{8}$$

This form can be further simplified using $G_{ij} = \exp(-\alpha_{ij}\tau_{ij})$ and $x_2 = 1 - x_1$ giving the following equation:

$$P_1 = P_1^{sat}x_1\exp\left((1 - x_1)^2\left(\tau_{21}\left(\frac{\exp(-\alpha_{21}\tau_{21})}{x_1 + (1 - x_1)\exp(-\alpha_{21}\tau_{21})}\right)^2 + \frac{\tau_{12}\exp(-\alpha_{12}\tau_{12})}{(1 - x_1 + x_1\exp(-\alpha_{12}\tau_{12}))^2}\right)\right) \tag{9}$$

with $\tau_{12} = b_{12} + c_{12}/T$ and $\tau_{21} = b_{21} + c_{21}/T$.

The parameters α_{ij}, b_{ij}, and c_{ij} were determined by fitting the solubility data of all isotherms to eq 9 using a least-squares method. The parameters are provided in Table 2.

The model correlations for $[C_4C_1im][OAc]$ and $[C_4C_1im][Cl]$ are shown in Figures 4a and 5a. This study only measured two temperatures for the $[C_2C_1im][BF_4]$ system; therefore, the solubility data for water in $[C_2C_1im][BF_4]$ at temperatures of 283, 291, 298, and 303 K were obtained from Takamuku et al.[13] and correlated with the NRTL model. Overall, the NRTL

Table 2. Binary NRTL Parameters of Water Vapor Solubility in Ionic Liquids

ionic liquid	α	b_{12}	c_{12} (K)	b_{21}	c_{21} (K)	S^a (kPa)	n^a
$[C_4C_1im][OAc]$	0.16	6.76	−122.00	−5.82	−388.00	0.05	39
$[C_4C_1im][Cl]$	0.32	7.05	−3009.51	−2.25	−201.01	<0.01	33
$[C_2C_1im][BF_4]$	0.82	13.53	−3139.19	−0.86	271.61	0.04	149

[a] S is the standard error of regression, and n is the number of data points fitted. Details can be found in the Supporting Information.

DOI: 10.1021/acs.iecr.8b05689
Ind. Eng. Chem. Res. 2019, 58, 1743−1753

model provides an excellent fit for all three systems as shown by the low standard errors of regression in Table 2. Considering that α is a measure of nonrandomness, and α = 0 describes the ideal random system, it can be concluded that the most nonideal system is $[C_2C_1im][BF_4]$ with α = 0.82. The nonrandom dispersion of water molecules in both $[C_2C_1im][BF_4]$[13] and $[C_4C_1im][BF_4]$[16] as described in the literature may provide some explanation for this nonideal behavior.

The NRTL τ_{ij} values (see the Supporting Information) calculated by the b_{ij} and c_{ij} parameters can also provide interesting conclusions on the energies of interaction for each water−IL system. Equation 10 illustrates the relationship between τ_{ij} and the energy interaction parameters g_{ij}.

$$\tau_{ij} = \frac{\Delta g_{ij}}{RT} = \frac{g_{ij} - g_{jj}}{RT} \quad (10)$$

The τ_{21} results for $[C_2C_1im][BF_4]$, $[C_4C_1im][OAc]$, and $[C_4C_1im][Cl]$ were ∼0.05, ∼−7.10, and ∼−2.91 as shown in Tables S10−S12 in the Supporting Information. It is important to consider that g_{ij} values are negative because they are attractive forces.[19] In the $[C_4C_1im][OAc]$ and $[C_4C_1im][Cl]$ systems the IL−water interactions $|g_{21}|$ (=$|g_{12}|$) are larger than the water−water interactions $|g_{11}|$, but in $[C_2C_1im][BF_4]$ the IL−water interactions are essentially the same to slightly weaker than the water−water energy interactions. This comparison suggests that substantial water−water bonding interactions exist in the $[C_2C_1im][BF_4]$ system which are energetically equal to, if not stronger than, the bonding occurring between water and the IL molecules. The τ_{21} values also show that the water solubility in ILs is dependent on the relative difference between the IL−water interactions and the IL−IL interactions. For example, the high water solubility in $[C_4C_1im][OAc]$ is due to the stronger IL−water interactions compared to the water−water interactions (i.e., low τ_{21} value). Higher τ_{21} values indicate a lower water solubility; for example, $[C_4C_1im][Cl]$ ($\tau_{21} \sim -2.91$) has a lower water solubility than $[C_4C_1im][OAc]$ ($\tau_{21} \sim -7.10$), followed by $[C_2C_1im][BF_4]$ ($\tau_{21} \sim 0.05$), which has an even lower water solubility.

III.c. Heats of Absorption. A comparison between the heat of absorption of water in the water−IL systems and the heat of vaporization of water can provide insight into the interaction behavior.[13] The heats of absorption for all three systems were calculated with the Clausius−Clapeyron equation, where the pressure values used were determined with the NRTL correlation at the temperatures measured (see the Supporting Information). The enthalpies of absorption calculated by Takamuku et al.[13] were recalculated in this work using their data and our NRTL model parameters.

The heats of water absorption as a function of water concentration in $[C_2C_1im][BF_4]$, $[C_4C_1im][OAc]$, and $[C_4C_1im][Cl]$ were compared to the enthalpy of vaporization for water (ΔH_{vap}) at 298.15 K (44 kJ/mol)[20] as shown in Figure 7. It is clear from Figure 7a that the IL−water interactions (i.e., heats of absorption) in the $[C_2C_1im][BF_4]$ system are weaker at lower concentrations of water (x_w); however, as the water concentration increases, the interactions with water increase and approach that of pure water−water interactions which are governed by hydrogen bonding. On the contrary, at low concentrations of water in $[C_4C_1im][OAc]$ and $[C_4C_1im][Cl]$ (Figure 7a,b), the heats of absorption are larger than the ΔH_{vap} of water, and as the water concentration increases, the interactions decrease and approach that of pure

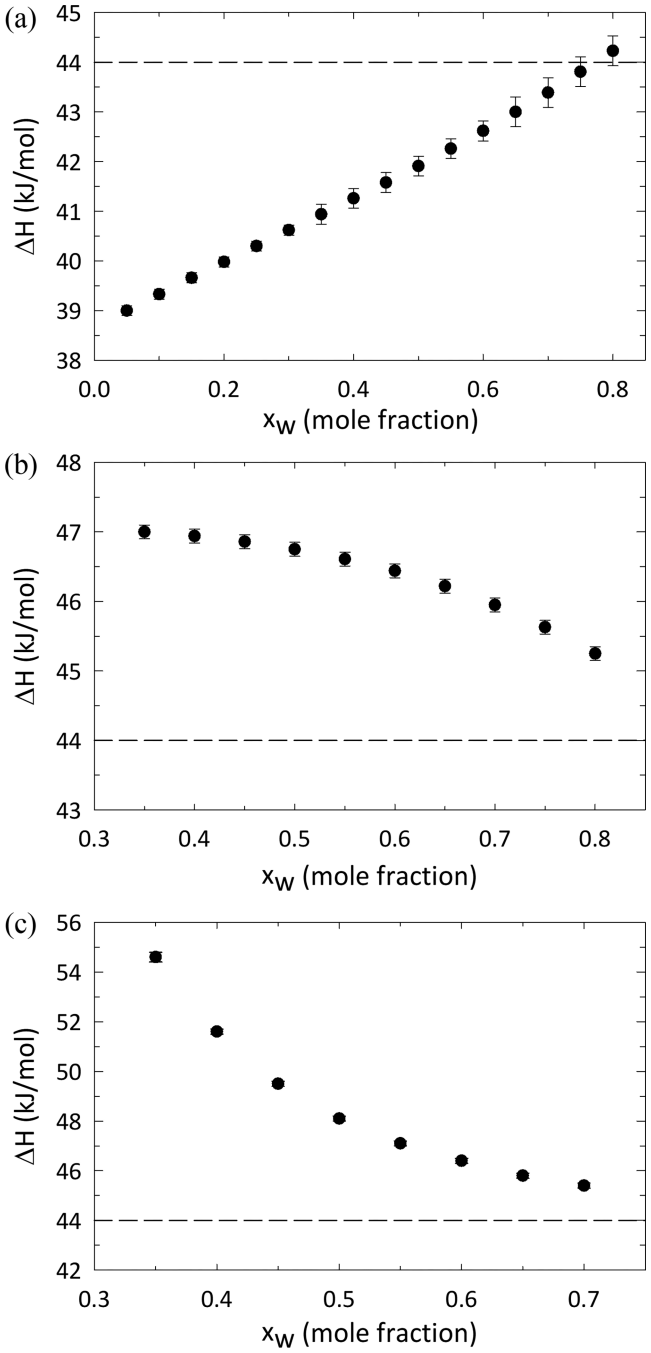

Figure 7. Enthalpy of absorption for water in (a) $[C_2C_1im][BF_4]$, (b) $[C_4C_1im][OAc]$, and (c) $[C_4C_1im][Cl]$. The standard errors are shown in vertical error bars. The dashed line represents the enthalpy of vaporization of water at 298 K.

water−water interactions. The energy interaction parameters g_{ij} suggested a similar behavior, where the IL−water interactions were shown to be slightly weaker than the water−water interactions in $[C_2C_1im][BF_4]$, but larger in $[C_4C_1im][OAc]$ and $[C_4C_1im][Cl]$. In addition, published activation energy (E_a) values for the rotational motion of water molecules in $[C_2C_1im][BF_4]$[13] and $[C_4C_1im][Cl]$[21] illustrate a similar trend. The E_a values suggest that an increase in water concentration increases the mobility of water molecules in $[C_4C_1im][Cl]$, but rather restricts the rotational motion of

DOI: 10.1021/acs.iecr.8b05689
Ind. Eng. Chem. Res. 2019, 58, 1743−1753

water in $[C_2C_1im][BF_4]$ (see the Supporting Information for additional details).

III.d. Diffusion. The mass absorption and desorption of water into the ionic liquid were measured as a function of time at each T and % RH; therefore, it was possible to calculate an effective binary diffusion coefficient. Due to the spherical shape of the Pyrex container, the ionic liquid volume was also a partial spherical shape (shown in Figure 8), where the water

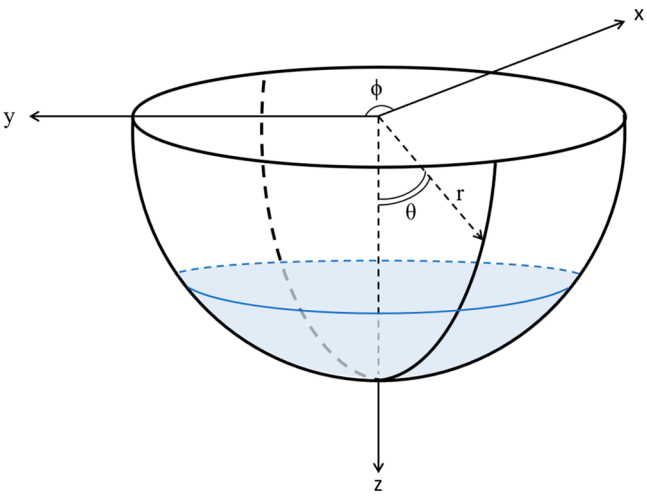

Figure 8. Partial spherical structure of the ionic liquid sample volume shown in the shaded region.

vapor is present above the partial sphere and enters the ionic liquid through the planar face. Water diffuses within the IL in radial and polar (θ) directions, and the concentration of water is equal across the azimuthal (ϕ) coordinate and symmetrical at $\theta = 0$. Finally, the diffusion stops at the walls of the glass bulb where the flux boundary condition is equal to zero. To simplify the calculation of the diffusion coefficient, the following assumptions were made:

- no convective force is present
- temperature and pressure remain constant at the specified set point
- the ionic liquid−water system is a dilute solution where thermophysical properties, such as density and viscosity, remain constant at the specified set point

The partial spherical shape of the ionic liquid in the sample container complicates the coordinate description of the top boundary condition, where the concentration of water is assumed to instantly reach the saturation concentration. For this reason, COMSOL Multiphysics modeling software was used to simulate the diffusion of water into a partial sphere of ionic liquid using Fick's law of diffusion, where C is the concentration of water (mol/m^3), t is time (s), and D is the diffusion coefficient (m^2/s) of water vapor in the IL:

$$\frac{\partial C}{\partial t} = D\nabla C \tag{11}$$

The geometry of COMSOL was defined by creating half of a two-dimensional (2D) hemisphere with radius = 6.37 mm (equal to the radius of the Pyrex sample container), and removing part of it to make the height (boundary 1 in Figure 9) equal to the height of the ionic liquid. This height was determined using eq 12, where the mass m (g), density ρ (g/cm^3), and radius r (cm) were known.

$$\frac{m}{\rho} = \frac{1}{3}\pi h^2(3r - h) \tag{12}$$

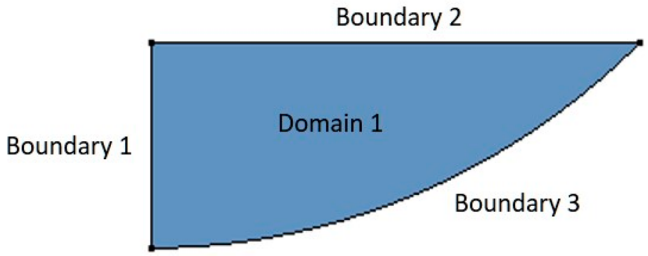

Figure 9. COMSOL 2D geometry with the domain and boundaries of interest.

The COMSOL Multiphysics software describes the entire geometry of the liquid by revolving the 2D shape in Figure 9 around the line $r = 0$ (boundary 1), thus creating a three-dimensional (3D) shape. The initial concentration (eq 13) was applied by setting an initial value condition to domain 1. The saturation condition (eq 14) can also be applied by setting a concentration condition for boundary 2 to equal C_s. The symmetry condition (eq 15) was applied using the "Axial Symmetry" condition for boundary 1. Finally, the no-flux boundary condition (eq 16) was set as boundary 3.

$$C = C_0 \quad \text{throughout the IL when } t = 0 \tag{13}$$

$$C = C_s \quad \text{at the top boundary when } t > 0 \tag{14}$$

$$\frac{\partial C}{\partial \theta} = 0 \quad \text{at } \theta = 0 \tag{15}$$

$$\frac{\partial C}{\partial r} = 0 \quad \text{at } r = R \tag{16}$$

Three methods were considered in the COMSOL Multiphysics analysis (see the Supporting Information), where the chosen approach was to use the COMSOL Multiphysics Optimization interface to solve for D, C_s, and C_0 while minimizing the sum of square differences between the simulation measurements and the experimental (mass fraction vs time) data (see details in the Supporting Information). This approach was applied to the time-dependent solubility data for the H_2O + $[C_4C_1im][OAc]$ system at 294.85 K and 15.67% RH, as reported in Table 3.

It was also desired to observe if the 1D diffusion approximation previously used by Minnick et al.[11] could be successfully used to predict the diffusion in this hemispherical system. The 1D diffusion approximation is shown in eq 17:

Table 3. D, C_s, and C_0 Determined by the 2D COMSOL Simulation and the 1D Diffusion Equation (eq 17) for the Solubility of Water in $[C_4C_1im][OAc]$ at 15.67% RH and 294.85 K

method	D ($\times 10^{-11}$ m^2/s)	C_s (wt %)	C_0 (wt %)	S^a (wt %)	n^a
measured	–	18.6	15.4	–	–
2D simulation	1.1	19.2	14.9	0.1	47
1D equation	1.1	18.6	15.0	0.1	47

[a] S is the standard error of regression, and n is the number of data points fitted. Details can be found in the Supporting Information.

DOI: 10.1021/acs.iecr.8b05689
Ind. Eng. Chem. Res. 2019, 58, 1743−1753

$$\langle C\rangle = C_s\left[1 - 2\left(1 - \frac{C_0}{C_s}\right)\sum_{n=0}^{\infty}\frac{\exp(-\lambda_n{}^2 Dt)}{L^2\lambda_n{}^2}\right] \quad (17)$$

which describes the average concentration of water $\langle C\rangle$ as a function of time for an ionic liquid system with height L in a cylindrical container, where $\lambda_n = (n + 1/2)\pi/L$. In this case the water vapor enters the system through the top flat face and travels downward in the z-direction. It is important to note that L in eq 17 is not equal to h from eq 12. The radius of the cylinder was assumed to be equal to the partial radius (i.e., the length of boundary 2 in Figure 9) calculated in eq 18, and the height (L) of the theoretical cylinder was calculated using eq 19, where the mass m (g), density ρ (g/cm^3), and radius r (cm) were known.

$$r_p = \sqrt{h(2r - h)} \quad (18)$$

$$L = \frac{m}{\rho\pi r_p{}^2} \quad (19)$$

In eq 17, 150 summations were used because additional terms had an impact of less than 1×10^{-14} (m^2/s) on the D coefficient and less than 1×10^{-4} (mass fraction) on the C_s and C_0 values. Figure 10 depicts the different fits obtained by

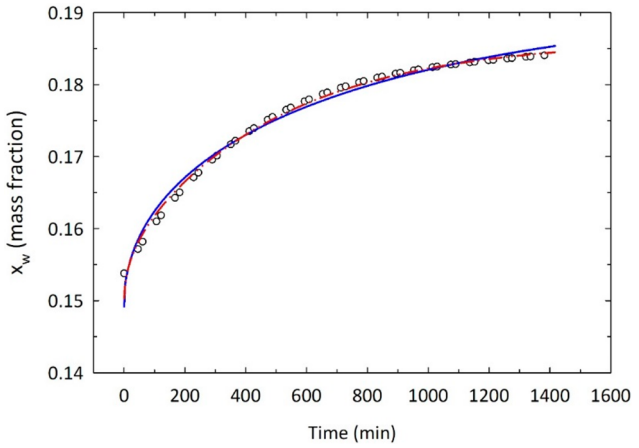

Figure 10. Comparison between using the COMSOL 2D mass transfer simulation fit (solid blue line) and the 1D diffusion equation (eq 17) (dotted−dashed red line) to determine the binary diffusion coefficient for water in ionic liquids by fitting the mass fraction per time data (open circles) of water−[C_4C_1im][OAc] system at 294.85 K and 15.67% RH.

the 1D diffusion equation, and Table 3 provides the values for D, C_s, C_0, and standard errors of regression (S). The 1D approximation, eq 17, was applied to the experimental concentration data using three methods (see the Supporting Information), and the chosen method fitted eq 17 to the mass fraction vs time data and determined the D, C_s, and C_0 values.

The results predicted by COMSOL Multiphysics and the 1D diffusion model are not significantly different, as shown in Figure 10 and Table 3; however, the 1D model predicts a C_s value closer to the measured water solubility. Therefore, the 1D model was used for the remainder of this study. In the future, a study comparing the two water absorption measurement techniques using the spherical and cylindrical shaped containers to evaluate differences in diffusion coefficients is recommended.

The concentration of water increases as RH increases; therefore, the physical properties of the system are not constant. Due to volume expansion, the height of the sample through which the water molecules must travel increases with increasing RH. A simple comparison was performed on the maximum RH measured to determine the difference between using a "dry" height (where the height is only due to the dry IL) and the average "wet" height due to volume expansion with water (see the Supporting Information for more details). The diffusion coefficients at the highest RH values were about 15% higher for [C_2C_1im][BF_4], 33% higher for [C_4C_1im][OAc], and 25% higher for [C_4C_1im][Cl], when using the average "wet" height, than when using the "dry" height in eq 17. For this reason, the diffusion coefficients calculated in this work use an average height at each T and % RH set point, where the average height is determined based on the initial height and final height at the specific set point (see the Supporting Information for more details). The diffusion coefficients determined using the 1D model and the average height approach are shown in Figures 11−13. The measured and calculated solubility of water using the 1D diffusion model can be found in the Supporting Information.

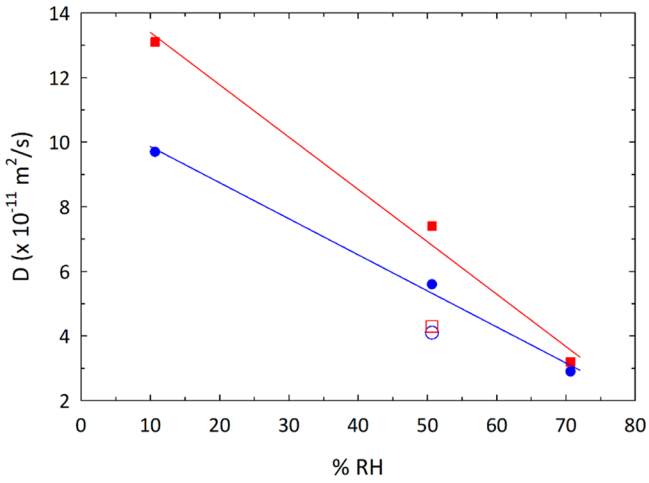

Figure 11. Diffusion results for absorption and desorption of water in [C_2C_1im][BF_4] determined using the 1D diffusion approximation. The blue circles represent data at 298.15 K, and red squares represent data at 303.15 K. The filled symbols are absorption, and empty symbols are desorption. Lines show trend. The uncertainties are T = ±0.01 K; % RH = ±1%; and $D \leq \pm 0.3 \times 10^{-11}$ m^2/s. Tabulated data can be found in the Supporting Information.

The reported diffusion coefficients for [C_2C_1im][BF_4], [C_4C_1im][OAc], and [C_4C_1im][Cl] increase with an increase in temperature, as expected. For example, the water absorption in [C_2C_1im][BF_4] at 10% RH and 298 K had $D = (9.7 \pm 0.1) \times 10^{-11}$ m^2/s, while at 303 K, $D = (13.1 \pm 0.1) \times 10^{-11}$ m^2/s. The 35% increase in the diffusion coefficient is due to the decrease in viscosity of the ionic liquid (0.0372 ± 0.0032 Pa·s at 298.15 K and 0.0314 ± 0.0021 Pa·s at 303.15 K)[22] which leads to faster water diffusion into the ionic liquid.

Also as expected, the viscosities of [C_2C_1im][BF_4], [C_4C_1im][OAc], and [C_4C_1im][Cl] decrease as the water concentration increases.[22−24] Therefore, diffusivity is expected to increase as relative humidity increases, and this was observed for [C_4C_1im][OAc] and [C_4C_1im][Cl]. Surprisingly, despite a decrease in viscosity as relative humidity increases,

DOI: 10.1021/acs.iecr.8b05689
Ind. Eng. Chem. Res. 2019, 58, 1743−1753

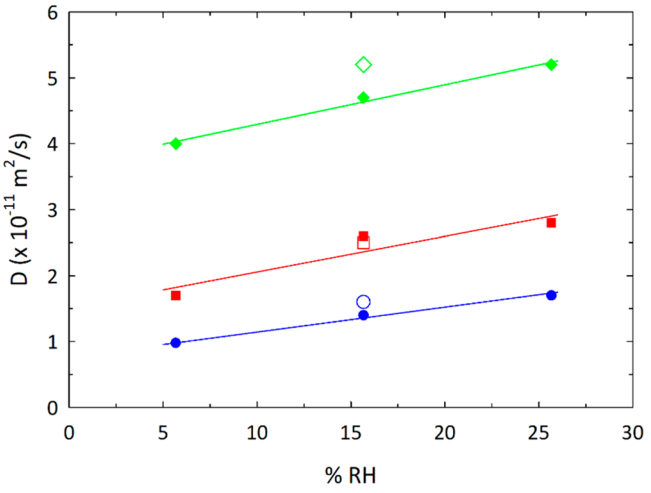

Figure 12. Diffusion results for absorption and desorption of water in $[C_4C_1im][OAc]$ determined using the 1D diffusion approximation. The blue circles represent data at 294.85 K, red squares represent data at 303.15 K, and green diamonds represent data at 315.15 K. The filled symbols are absorption, and empty symbols are desorption. Lines show trend. The uncertainties are T = ±0.01 K; % RH = ±1%; and D < 0.2 × 10^{-11} m^2/s. Tabulated data can be found in the Supporting Information.

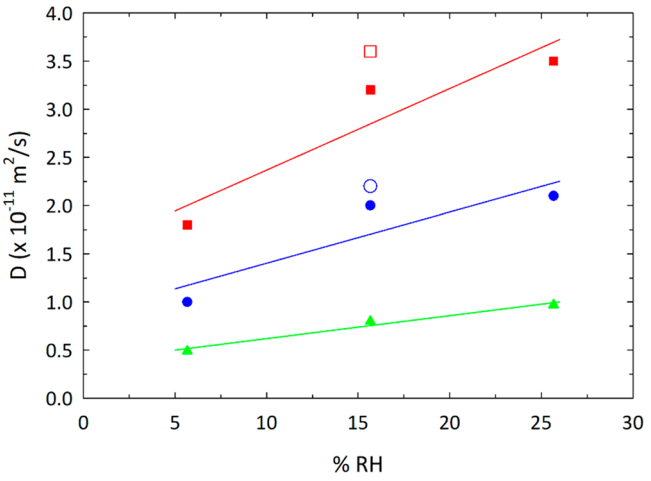

Figure 13. Diffusion results for absorption and desorption of water in $[C_4C_1im][Cl]$ determined using the 1D diffusion approximation. The green triangles represent data at 283.15 K, blue circles represent data at 295.15 K, and red squares represent data at 303.15 K. The filled symbols are absorption, and empty symbols are desorption. Lines show trend. The uncertainties are T = ±0.01 K; % RH = ±1%; and D < 0.2 × 10^{-11} m^2/s. Tabulated data can be found in the Supporting Information.

the H_2O + $[C_2C_1im][BF_4]$ system shows a decrease in diffusion D. The desorption coefficients for the $[C_4C_1im][OAc]$ and $[C_4C_1im][Cl]$ were not significantly different from the absorption diffusion coefficients, but in general the desorption D values were slightly higher. This is expected because the diffusion during the desorption process begins with a higher water concentration; therefore, the viscosity is lower than the corresponding absorption process at the same T and P conditions. However, in the case of $[C_2C_1im][BF_4]$ the desorption coefficients were lower than the absorption coefficients; for example, at 298.15 K and 50.67% RH, $D_{desorption}$= (4.1 ± 0.2) × 10^{-11} m^2/s vs $D_{absorption}$ = (5.6 ± 0.1) × 10^{-11} m^2/s. This again illustrates the unexpected influence the presence of water has on the diffusion coefficient in $[C_2C_1im][BF_4]$.

III.e. Stokes–Einstein Estimation of Diffusing Radius.

A comparison of the diffusing radii in the IL–water systems may also provide insight regarding the difference in diffusion coefficients of such systems. The Stokes–Einstein equation provides the relationship of a spherical solute A with radius r_A diffusing through a solution B with viscosity η_B, as shown in eq 20, where k is the Boltzmann constant.

$$D = \frac{kT}{6\pi r_A \eta_B} \tag{20}$$

This equation was modified empirically by Shiflett and Yokozeki[25] to introduce the dependence of diffusion on the mixture density raised to a power b (i.e., $D \propto \eta^{-b}$), and it is shown in eq 21, where a normalization factor was included (η_0 = 1 mPa·s) and $a = \ln(k/6\pi r\eta_0)$.

$$\ln(D/T) = a - b\ln(\eta/\eta_0) \tag{21}$$

The diffusion data as a function of T and x_w were fit with eq 21 along with viscosity data determined from the literature to calculate the diffusing radius, r, in coefficient a. The resulting diffusing radius for the water–$[C_4C_1im][OAc]$ and water–$[C_4C_1im][Cl]$ systems were ∼1 nm, and >15 nm for the water–$[C_2C_1im][BF_4]$ system. The radii of water, $[OAc]^-$, $[Cl]^-$, and $[BF_4]^-$ are 0.14,[26] 0.16,[27] 0.18,[28] and 0.22 nm,[29] respectively. This supports the hypothesis that $[C_4C_1im][OAc]$ and $[C_4C_1im][Cl]$ ionic liquids coordinate with only a few water molecules through hydrogen bonding, and that much larger water/BF_4^- clusters/networks are occurring in the $[C_2C_1im][BF_4]$ system, where water–water hydrogen bonds form and may aggregate with or around BF_4 ions. Several studies agree on the possibility that water aggregates and ionic clusters may form in aqueous IL mixtures.[2,30−33] Therefore, although viscosity of the water–IL systems decreased as water concentration increased, the size of the diffusing species in

Table 4. Comparison of Diffusion Coefficients and ΔH_{abs} of Water in $[C_2C_1im][BF_4]$, $[C_4C_1im][OAc]$, and $[C_4C_1im][Cl]$ as a Function of Temperature and Viscosity

ionic liquid	T^a (K)	$x_w{}^a$ (mol %)	μ^b (Pa·s)	D (m^2/s)	ΔH_{abs} (kJ/mol)
$[C_2C_1im][BF_4]$	298.15	8.45	0.030	(9.7 ± 0.1) × 10^{-11}	39.2 ± 0.1
	303.15	9.23	0.025	(13.1 ± 0.1) × 10^{-11}	39.3 ± 0.1
$[C_4C_1im][OAc]$	294.85	77.8	0.039	(1.7 ± 0.1) × 10^{-11}	45.4 ± 0.1
	303.15	78.1	0.024	(2.8 ± 0.1) × 10^{-11}	45.4 ± 0.1
$[C_4C_1im][Cl]$	295.15	69.3	0.040	(2.1 ± 0.1) × 10^{-11}	45.5 ± 0.1
	303.15	69.0	0.028	(3.5 ± 0.1) × 10^{-11}	45.5 ± 0.1

[a]The uncertainties are T ± 0.01 K and x_w < 0.1 mol % . [b]The viscosity values for $[C_2C_1im][BF_4]$,[22] $[C_4C_1im][OAc]$,[23] and $[C_4C_1im][Cl]$[24] were determined from the literature.

DOI: 10.1021/acs.iecr.8b05689
Ind. Eng. Chem. Res. 2019, 58, 1743−1753

$[C_2C_1im][BF_4]$ is expected to increase whereas the diffusing radii in the $[C_4C_1im][OAc]$ and $[C_4C_1im][Cl]$ are expected to remain constant.

III.f. Relationship between the Heat of Absorption and the Diffusion Coefficient. The effect of the water−IL interactions on the diffusion coefficients are clearly observed when comparing the three systems at similar viscosities and temperatures as shown in Table 4. The ΔH_{abs} of water and viscosity in $[C_4C_1im][OAc]$ (45.4 ± 0.1 kJ/mol, 0.024 Pa·s, x_w = 78.1 mol %) and $[C_4C_1im][Cl]$ (45.5 ± 0.1 kJ/mol, 0.028 Pa·s, x_w = 69.0 mol %) at 303.15 K were essentially the same; therefore, the absorption diffusions were similar ($D_{[C_4C_1im][OAc]}$ = (2.8 ± 0.1) × 10^{-11} m^2/s and $D_{[C_4C_1im][Cl]}$ = (3.5 ± 0.1) × 10^{-11} m^2/s). However, at the same conditions (0.025 Pa·s), the H_2O + $[C_2C_1im][BF_4]$ system (at x_w = 9.23 mol %) had a lower ΔH_{abs} of water (39.3 ± 0.1 kJ/mol) and a significantly higher absorption diffusion (13.1 × 10^{-11} m^2/s). The same behavior is also observed at 294.85−298.15 K and 0.030−0.041 Pa·s, as shown in Table 4. Therefore, the measurements indicate that, even though the viscosity of all three IL−water systems decreases as water concentration increases, the diffusion coefficients are also a function of the molecular (water−water and water−IL) interactions (i.e., ΔH_{abs}). To better understand the interaction behavior of water molecules with the IL cations and anions, a molecular simulation study is recommended. The use of molecular simulations could provide further insights into the structure and state of water in these interesting IL−water systems.

IV. CONCLUSION

The solubility of water was measured in three ionic liquids ($[C_2C_1im][BF_4]$, $[C_4C_1im][OAc]$, and $[C_4C_1im][Cl]$) using an IGAsorp gravimetric microbalance over a range of temperature (293−315 K) and relative humidity (0−70%). The solubility of water in $[C_2C_1im][BF_4]$ agreed with published data and provided confidence that the method was reliable for measuring water sorption in ionic liquids. The solubility of water was the highest in $[C_4C_1im][OAc]$ (77.5 mol %), followed by $[C_4C_1im][Cl]$ (68.6 mol %) and $[C_2C_1im][BF_4]$ (19.5 mol %) at equivalent conditions (303.15 K and 25% RH).

The activity coefficient NRTL model was successfully used to correlate the solubility data of the three IL systems. Temperature independent parameters were calculated using the solubility for each isotherm. Furthermore, energy interaction parameters (α, τ_{12}, and τ_{21}) provided further explanation for the solubility differences observed between $[C_4C_1im][OAc]$, $[C_4C_1im][Cl]$, and $[C_2C_1im][BF_4]$.

A diffusion analysis was performed using two different models: one which considered the 2D diffusion behavior in a partial hemisphere, and another which applied the 1D diffusion equation employed in previous works.[11] This work demonstrated the 1D diffusion model provides satisfactory predictions and can be used to determine the water−IL binary coefficients. Upon comparing the diffusion coefficients, the expected increase in diffusion with lower viscosity as temperature increases was confirmed for the three water−IL systems. However, an unexpected result was observed for $[C_2C_1im][BF_4]$ with the decrease in diffusion (from 13.1 × 10^{-11} to 3.2 × 10^{-11} m^2/s) as water concentration increased (i.e., lower viscosity), whereas the expected result, an increase in diffusion with increasing water content, was observed for $[C_4C_1im][OAc]$ (from 1.7 × 10^{-11} to 2.8 × 10^{-11} m^2/s) and $[C_4C_1im][Cl]$ (from 1.8 × 10^{-11} to 3.5 × 10^{-11} m^2/s). Diffusing radius calculations using the Stokes−Einstein relationship support the hypothesis that only a few water molecules through hydrogen bonding form clusters with the [OAc] and [Cl] anions, but much larger water/BF_4^- clusters/networks are occurring in the $[C_2C_1im][BF_4]$ system which increase in size with increase in water concentration.

The NRTL correlations and the Clausius−Clapeyron equation were used to determine the enthalpy of absorption for the three ILs, which were compared to the water−water interactions illustrated by the heat of vaporization of water at 298 K. This assessment, along with rotational energy information and the NRTL interaction parameters, also provides further support for the differences observed in the diffusivity of water in each IL. In general, $[C_2C_1im][BF_4]$ displays weaker interactions with water than $[C_4C_1im][OAc]$ and $[C_4C_1im][Cl]$. It was observed that, as water concentration increased, the water−water hydrogen bonding energy began to exceed the $[C_2C_1im][BF_4]$−water interactions, and the water diffusivity decreased. On the other hand, the increase in water concentration in $[C_4C_1im][OAc]$ and $[C_4C_1im][Cl]$ decreased the interactions between water−IL, and was presumed to increase water mobility; therefore, the water diffusivity increased.

■ ASSOCIATED CONTENT

Supporting Information

The Supporting Information is available free of charge on the ACS Publications website at DOI: 10.1021/acs.iecr.8b05689.

Water solubility and density data, NRTL modeling, enthalpy of absorption, diffusion modeling, diffusion coefficient data (PDF)

■ AUTHOR INFORMATION

Corresponding Author

*Tel.: (785) 864-6719. E-mail: mark.b.shiflett@ku.edu.

ORCID

M. Alejandra Rocha: 0000-0002-7743-6692

Mark B. Shiflett: 0000-0002-8934-6192

Notes

The authors declare no competing financial interest.

■ ACKNOWLEDGMENTS

The authors would like to thank Dr. Kevin Leonard at the University of Kansas for his guidance in using COMSOL Multiphysics, and Tugba Turnaoglu at the University of Kansas for providing the source MATLAB code for the 1D diffusion equation. The authors would also like to thank Dr. Mark Roper, Katherine McKie, and Mathew Powner at Hiden Isochema for their attentive instrument support, and Mo Akhtar for installation support.

■ ABBREVIATIONS

IL = ionic liquid

$[C_2C_1im][BF_4]$ = 1-ethyl-3-methylimidazolium tetrafluoroborate

$[C_4C_1im][OAc]$ = 1-butyl-3-methylimidazolium acetate

$[C_4C_1im][Cl])$ = 1-butyl-3-methylimidazolium chloride

DOI: 10.1021/acs.iecr.8b05689
Ind. Eng. Chem. Res. 2019, 58, 1743−1753

REFERENCES

(1) Lei, Z.; Chen, B.; Koo, Y.-M.; MacFarlane, D. R. Introduction: Ionic Liquids. *Chem. Rev.* **2017**, *117*, 6633−6635.
(2) Kohno, Y.; Ohno, H. Ionic Liquid/Water Mixtures: From Hostility to Conciliation. *Chem. Commun.* **2012**, *48*, 7119−7130.
(3) Kelkar, M. S.; Maginn, E. J. Effect of Temperature and Water Content on the Shear Viscosity of the Ionic Liquid 1-Ethyl-3-Methylimidazolium Bis(Trifluoromethanesulfonyl)Imide as Studied by Atomistic Simulations. *J. Phys. Chem. B* **2007**, *111*, 4867−4876.
(4) Seddon, K. R.; Stark, A.; Torres, M.-J. Influence of Chloride, Water, and Organic Solvents on the Physical Properties of Ionic Liquids*. *Pure Appl. Chem.* **2000**, *72*, 2275−2287.
(5) Pei, Y.; Wang, J.; Wu, K.; Xuan, X.; Lu, X. Ionic Liquid-Based Aqueous Two-Phase Extraction of Selected Proteins. *Sep. Purif. Technol.* **2009**, *64*, 288−295.
(6) Swatloski, R. P.; Spear, S. K.; Holbrey, J. D.; Rogers, R. D. Dissolution of Cellose with Ionic Liquids. *J. Am. Chem. Soc.* **2002**, *124*, 4974−4975.
(7) O'Mahony, A. M.; Silvester, D. S.; Aldous, L.; Hardacre, C.; Compton, R. G. Effect of Water on the Electrochemical Window and Potential Limits of Room-Temperature Ionic Liquids. *J. Chem. Eng. Data* **2008**, *53*, 2884−2891.
(8) Maiti, A.; Kumar, A.; Rogers, R. D. Water-Clustering in Hygroscopic Ionic Liquids - An Implicit Solvent Analysis. *Phys. Chem. Chem. Phys.* **2012**, *14*, 5139−5146.
(9) Welton, T. Ionic Liquids in Catalysis. *Coord. Chem. Rev.* **2004**, *248*, 2459−2477.
(10) Holbrey, J. D.; Reichert, M. M.; Nieuwenhuyzen, M.; Sheppard, O.; Hardacre, C.; Rogers, R. D. Liquid Clathrate Formation in Ionic Liquid-Aromatic Mixtures. *Chem. Commun.* **2003**, *3*, 476−477.
(11) Minnick, D. L.; Turnaoglu, T.; Rocha, M. A.; Shiflett, M. B. Review Article: Gas and Vapor Sorption Measurements Using Electronic Beam Balances. *J. Vac. Sci. Technol., A* **2018**, *36*, 050801.
(12) Lemmon, E. W.; Huber, M. L.; Mclinden, M. O. *REFPROP 9.1. NIST Standard Reference Database*; National Institute of Standards and Technology: 2013.
(13) Takamuku, T.; Kyoshoin, Y.; Shimomura, T.; Kittaka, S.; Yamaguchi, T. Effect of Water on Structure of Hydrophilic Imidazolium-Based Ionic Liquid. *J. Phys. Chem. B* **2009**, *113*, 10817−10824.
(14) Finotello, A.; Bara, J. E.; Camper, D.; Noble, R. D. Room-Temperature Ionic Liquids: Temperature Dependence of Gas Solubility Selectivity. *Ind. Eng. Chem. Res.* **2008**, *47*, 3453−3459.
(15) Anderson, J. L.; Dixon, J. K.; Brennecke, J. F. Solubility of CO2, CH4, C2H6, C2H4, O2, and N2 in 1-Hexyl-3-Methylpyridinium Bis(Trifluoromethylsulfonyl)Imide: Comparison to Other Ionic Liquids. *Acc. Chem. Res.* **2007**, *40*, 1208−1216.
(16) Dahi, A.; Fatyeyeva, K.; Chappey, C.; Langevin, D.; Rogalsky, S. P.; Tarasyuk, O. P.; Marais, S. Water Sorption Properties of Room-Temperature Ionic Liquids over the Whole Range of Water Activity and Molecular States of Water in These Media. *RSC Adv.* **2015**, *5*, 76927−76938.
(17) Zhao, J.; Jiang, X.-C.; Li, C.-X.; Wang, Z.-H. Vapor Pressure Measurement for Binary and Ternary Systems Containing a Phosphoric Ionic Liquid. *Fluid Phase Equilib.* **2006**, *247*, 190−198.
(18) Wang, J.-F.; Li, C.-X.; Wang, Z.-H.; Li, Z.-J.; Jiang, Y.-B. Vapor Pressure Measurement for Water, Methanol, Ethanol, and Their Binary Mixtures in the Presence of an Ionic Liquid 1-Ethyl-3-Methylimidazolium Dimethylphosphate. *Fluid Phase Equilib.* **2007**, *255*, 186−192.
(19) Belvèze, L. S. *Modeling and Measurement of Thermodynamic Properties of Ionic Liquids*. Master's Thesis, University of Notre Dame, 2004.
(20) Haywood, R. *Thermodynamic Tables in SI (Metric) Units*; Cambridge University Press: London, 1972.
(21) Yasaka, Y.; Wakai, C.; Matubayasi, N.; Nakahara, M. Rotational Dynamics of Water and Benzene Controlled by Anion Field in Ionic Liquids: 1-Butyl-3-Methylimidazolium Chloride and Hexafluorophosphate. *J. Chem. Phys.* **2007**, *127*, 104506.
(22) Zhang, S.; Li, X.; Chen, H.; Wang, J.; Zhang, J.; Zhang, M. Determination of Physical Properties for the Binary System of 1-Ethyl-3-Methylimidazolium Tetrafluoroborate + H_2O. *J. Chem. Eng. Data* **2004**, *49*, 760−764.
(23) Stevanovic, S.; Podgoršek, A.; Pádua, A. A. H.; Costa Gomes, M. F. Effect of Water on the Carbon Dioxide Absorption by 1-Alkyl-3-Methylimidazolium Acetate Ionic Liquids. *J. Phys. Chem. B* **2012**, *116*, 14416−14425.
(24) Yang, Q.; Yu, K.; Xing, H.; Su, B.; Bao, Z.; Yang, Y.; Ren, Q. The Effect of Molecular Solvents on the Viscosity, Conductivity and Ionicity of Mixtures Containing Chloride Anion-Based Ionic Liquid. *J. Ind. Eng. Chem.* **2013**, *19*, 1708−1714.
(25) Shiflett, M. B.; Harmer, M. A.; Junk, C. P.; Yokozeki, A. Solubility and Diffusivity of Difluoromethane in Room-Temperature Ionic Liquids. *J. Chem. Eng. Data* **2006**, *51*, 483−495.
(26) D'Arrigo, J. S. Screening of Membrane Surface Charges by Divalent Cations: An Atomic Representation. *Am. J. Physiol.* **1978**, *235*, C109−C117.
(27) Lovell, C. S.; Walker, A.; Damion, R. A.; Radhi, A.; Tanner, S. F.; Budtova, T.; Ries, M. E. Influence of Cellulose on Ion Diffusivity in 1-Ethyl-3-Methyl-Imidazolium Acetate Cellulose Solutions. *Biomacromolecules* **2010**, *11*, 2927−2935.
(28) Bondi, A. van der Waals Volumes and Radii. *J. Phys. Chem.* **1964**, *68*, 441−451.
(29) Wasserscheid, P.; Welton, T. *Ionic Liquids in Synthesis*, 2nd ed.; Wiley-VCH: 2008; Vol. *1*.
(30) Di Francesco, F.; Calisi, N.; Creatini, M.; Melai, B.; Salvo, P.; Chiappe, C. Water Sorption by Anhydrous Ionic Liquids. *Green Chem.* **2011**, *13*, 1712−1717.
(31) Reid, J. E. S. J.; Walker, A. J.; Shimizu, S. Residual Water in Ionic Liquids: Clustered or Dissociated? *Phys. Chem. Chem. Phys.* **2015**, *17*, 14710−14718.
(32) Chen, Y.; Sun, X.; Yan, C.; Cao, Y.; Mu, T. The Dynamic Process of Atmospheric Water Sorption in [EMIM][Ac] and Mixtures of [EMIM][Ac] with Biopolymers and CO2capture in These Systems. *J. Phys. Chem. B* **2014**, *118*, 11523−11536.
(33) Hall, C. A.; Le, K. A.; Rudaz, C.; Radhi, A.; Lovell, C. S.; Damion, R. A.; Budtova, T.; Ries, M. E. Macroscopic and Microscopic Study of 1-Ethyl-3-Methyl-Imidazolium Acetate-Water Mixtures. *J. Phys. Chem. B* **2012**, *116*, 12810−12818.

NOTE ADDED AFTER ASAP PUBLICATION

This paper was published on the Web on January 22, 2019, with RH value errors on page three of the document. The corrected version was reposted on January 30, 2019.

DOI: 10.1021/acs.iecr.8b05689
Ind. Eng. Chem. Res. 2019, 58, 1743−1753